SINGLE DEGREE OF FREEDOM ANALYSIS OF A TUNNEL LINER AND THE SOIL BEHIND IT

A Thesis

Presented to

The Faculty of the Department of Civil Engineering

California State University, Los Angeles

In Partial Fulfillment

of the Requirements for the Degree

Master of Science

in

Civil Engineering

By

Luis Alberto Sosa

August 2023

The thesis of Luis Alberto Sosa is approved.

Tonatiuh Rodriguez-Nikl, Committee Chair

Wing Shun Kwan

Maryam Nazari

Gustavo Menezes, Department Chair

California State University, Los Angeles

August 2023

ABSTRACT

Single degree of freedom analysis of a tunnel liner and the soil behind it

By

Luis Alberto Sosa

Understanding the response a tunnel will have when subjected to explosive loading has become an important topic. In recent years, concerns about potential accidents or attacks in tunnels and similar infrastructures has been escalating. Understanding of the factors that influence the tunnel's response and utilizing numerical models to test various scenarios that tunnels may encounter will provide valuable insights into effective damage mitigation strategies. Current models used to predict the maximum deformation of a tunnel liner are complicated and time consuming. The need for a different way to calculate this value led to the creation of a new theoretical model based on single degree of freedom methods and a corresponding numerical implementation. In this thesis I show that using a simplified single degree of freedom model with soil shows potential for producing quick results with good accuracy. Nevertheless, it is important to acknowledge that this model does have several limitations, which we have identified and will discuss in this thesis.

ACKNOWLEDGMENTS

This work was carried out with support from the University Transportation Center for Underground Transportation Infrastructure (UTC-UTI). The contents of this report reflect the views of the authors, who are responsible for the facts and the accuracy of the information presented herein. This document is disseminated in the interest of information exchange. The report is funded, partially or entirely, by a grant from the U.S. Department of Transportation's University Transportation Centers Program. However, the U.S. Government assumes no liability for the contents or use thereof.

TABLE OF CONTENTS

Contents

LIST OF TABLES

LIST OF FIGURES

Figure

CHAPTER 1

Existing Practice

Overview

Train tunnels are a key element in any transportation system that provides the public and country with convenient passageways. The Federal Highway Administration (FHWA; Roberts et al., 2003) stated that many countries' current transportation systems are under strain to keep up with demands of growing populations. Therefore, the need for trains and tunnels to stay functional is essential for a country's societal and economic stability. The FHWA also mentioned that transportation and related structures are attractive terrorist targets because of their accessibility and potential impact on human lives and economic activity. Zaghloul et al. (2018) mentioned that those who wish to cause harm to tunnels have ample ability to do so due to the high vulnerability that comes with unrestricted public access and the ease of transporting personnel borne improvised explosive devices (PBIEDs) through the transportation system. Knowing that one of the largest key elements of any transportation system is under the threat of terrorism the need to act becomes evident. One way to act is to understand how tunnels behave under the loads of blasts, which has been the study focus for many research papers including this one.

The first part of this chapter will be focusing on the review of relevant literature on a tunnel response to blast load and the second part will provide details about the Single Degree of Freedom (SDOF) method. Before introducing previous research, an explanation of concepts and terms that are related to tunnel construction and blast loading is required.

Fundamental Concepts in Blast Response of Tunnels

The tunnel shape refers to the cross-sectional shape of a tunnel. The three main cross-sectional shapes for tunnels are circular, horseshoe, and rectangular (Fig. 1). The magnitude of the cross-sectional width and height also play a role in the calculations because it affects factors such as the standoff distance, which is the distance from the charge is to an element. The tunnel liner supports the perimeter of a tunnel and consists of structural support pieces that are combined to form a complete tunnel passageway. Tunnel liners are mainly made up of steel and concrete. In some cases, tunnel liners can have additional materials that support the liner in areas such as damping, overall liner strength and other possible needs.

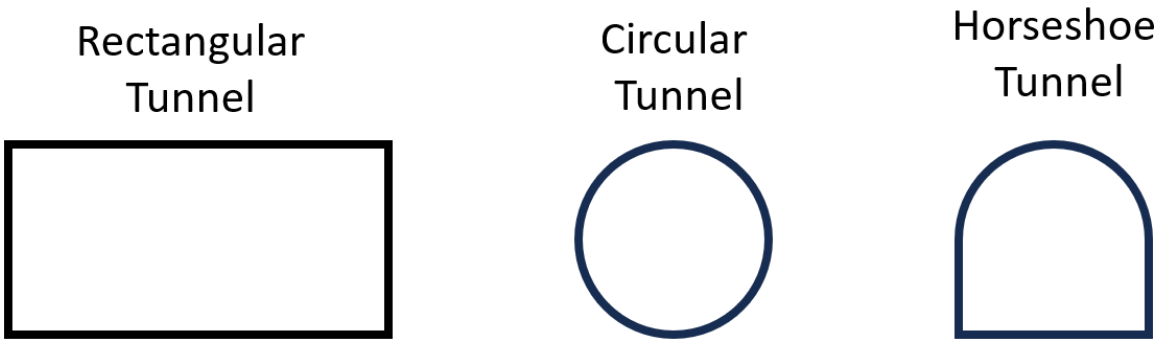

Figure 1: Tunnel Cross Sections

The second main set of terms used throughout this paper focuses on the explosives and concepts surrounding them. Improvised explosive devices (IEDs) are not conventional manufactured explosive like those used by the military. Instead, they are created using components that might have had non-explosive purpose but have been modified for use in creating explosives, often by terrorists or other individuals. Some IED

are classified as vehicle borne improvised explosive devices (VBIEDs), or car bombs. Others are classified as person borne improvised explosive devices (PBIEDs), which are much smaller in size because they are meant to be carried by a person but have the advantage of being able to be transported more easily. The size of the explosive is defined by its charge weight. Standoff distance is the distance from the center of the explosive to the building element under considerations. Spall and breach both describe local failure modes. Spall is used in this paper to describe areas in concrete which have cracked, chipped away, or flaked off due to a pressure exerted on it exceeding its strength. On the other hand, breach is used to describe that there has been a gap made in the wall. Tunnel liners can also have global failure modes such as bending moment or shear of the cross section. The last term we will introduce here is the scaled distance:

$$Z = \frac{R}{W^{\frac{1}{3}}} \tag{1}$$

In the equation Z represents the scaled distance, R represents the standoff distance from the center of the charge to the wall, and W is the weight of the explosive in terms of an equivalent weight of trinitrotoluene (TNT).

There are three types of methods used to predict the response of tunnels to blast loads: high-fidelity physics computer analysis programs, intermediate models, and single degree of freedom (SDOF) methods. In this thesis paper, we create and use a SDOF method because of its ease of use and quick assessment when compared to the more complicated high-fidelity analysis methods. The problem that motivated this thesis was the need for a quick method of analysis, in support of engineering design, to predict the maximum deformation of a curved tunnel liner subjected to a PBIED. As a first step, we are extending the current SDOF approach for a rectangular tunnel liner to include the soil

behind it. Additionally, we are also looking at a more conventional charge instead of PBIED. This was done because the existing methods are best suited to larger charges acting over the whole element. The focus of this paper is to see if the soil can be added to the SDOF model.

High-fidelity and intermediate studies on tunnel response

Choi et al. (2012) investigated the result of explosions on underground facilities using key factors including charge weight, tunnel size and shape, standoff distance, and various types of soil surrounding the tunnel. Choi et al. employed a three-dimensional coupled Euler-Lagrange nonlinear dynamic analysis using the computer program AUTODYN. The Euler part of the mesh models the pressure wave through the air, while the Lagrange part of the mesh models the structural elements. This differs from other methods where the pressure pulse is pre-defined and does not depend on how the structure behaves. Choi and colleagues created design charts for pressure, impulse, and other important parameters. However, these charts only cover a limited range of input values, so there remains a need for additional design-oriented results.

Bai et al. (2018) understood that the current methods for evaluating blast induced damage are either oversimplified in their approach or require significant computational effort. In response, they developed a simplified characterization of the tunnel response. For this study the parametric computer-aided design (CAD) environment was used to generate an extruded tunnel cross section and analyze its intersection with the blast-induced damage spheres. When these damage spheres interact with the tunnel, they indicate the extent of the breach and spall damage. The size of the spheres also represents the distance from the charge that breach and spall will occur. The spheres were computed

using a high-fidelity model, LS-DYNA, and used to compare the values from their proposed simplified approach. When comparing the two methods, Bai and colleagues found the overall areas of spall and breach were within 10% of each other, with the computational model indicating slightly more breach and the proposed approach slightly more spall.

Several other aspects of the response of tunnels to blast loads have been examined. Chakraborty et al. (2014) investigated the performance of different tunnel lining materials under the loading of an internal blast. Materials that were considered were a single layered steel plate, plain concrete (PC), a steel fiber reinforced concrete (SFRC) slab, sandwich steel-dytherm foam-steel (SDS) panel, and steel-polyurethane foam-steel (SPS) panel linings. To compare the different tunnel lining materials under blast loading, the finite element software Abaqus/Explicit was used to create the three-dimensional finite element models. The use of SDS as tunnel lining material resulted in the minimum peak displacement compared to all other material analyzed.

Ranjit et al. (2019) expanded on the work done by Chakraborty et al. (2014). Ranjit et al. used a three-dimensional finite element analysis method to compare the performance of conventional and advanced tunnel lining under blast loading. In this study the conventional tunnel lining materials are plain concrete, steel reinforced cement concrete (RC), and SFRC. The advanced tunnel lining material used for analysis were dytherm, polyurethane, and aluminum syntactic foam sandwich panels with steel–foam–steel composites. Ranjit et al. carried out the nonlinear three-dimensional finite element analysis of tunnel lining material using Abaqus 6.14. The authors summarized their findings and concluded that steel reinforced concrete minimized displacement the best

when compared to PC and SFRC. The best performers at minimizing deflection were the sandwich panels of the advanced tunnel lining material. These results supported those found by Chakraborty et al. (2014).

Zaghloul et al. (2018) shifted the focus from damage to the tunnel liner to the damage to the train carriages and its passengers. Their study simulated the blast effects inside train carriages in tunnels using the advanced finite element code LS-DYNA. The research focused on different charge sizes and charge locations to analyzing the effects each have on the carriages and its passengers. Their results concluded that there was a significant influence from the size of the charge and its location on the number and severity of injuries to the passengers. Almost every scenario gave the passengers some sort of bodily damage such as eardrum rupture, head impact, whole-body impact, and lung hemorrhage. These parameters also affected the peaks of pressure experienced by individuals in the carriage as a result of the initial blast wave hitting the wall of the tunnel and reflecting back onto those near the windows. Zaghloul and colleagues found that the pressure from the reflecting waves is smaller than the initial incidents pressure but the impulse is higher.

Feldgun et al. (2014) studied the effect an explosion in a rectangular tunnel would have on a neighboring buried structure and the surrounding soil. They studied five cases with varying charge location and distances between the tunnel structure and the nearby buried structure. Additionally, there was one case that did not consider a nearby buried structure. To analyze the behavior of the structure they used both analytical and numerical modeling. They used AUTODYN to model the blast loading acting on the surface of the tunnel lining. The results showed that the charge location significantly

affected the vertical peak velocity displacement and caused the maximum value of vertical displacement. In the case where the neighboring tunnel was absent caused minimum displacement, and was found to worsen the stress distribution along the rectangular tunnel.

Shin et al. (2011) studied the behavior of a horse-shoe shaped tunnel in soft rock under the effects of a blast. A two-dimensional numerical model was used for both the blast load and for the dynamic modeling of the tunnel in soft rock. Nine cases were analyzed, categorized into two groups, each focusing on different blast locations. Group 1 had five cases that varied the vertical location of the charge, while group 2 had four cases that varied the lateral location of the charge. The results from all these cases showed that the maximum particle velocity of the tunnel, maximum displacement, and stress all increased when standoff distance decreased. Shin and colleagues' results are based on a tunnel surrounded by soft rock, but with special consideration can be adapted for tunnels with different tunnel shape and ground conditions.

Han et al. (2016) studied the interaction between circular subway tunnels and saturated soils subjected to medium internal blast loads to improve the rehabilitation of transportation tunnels. They simulated the blast loading using LS-DYNA, while the time histories of the incident were derived from the embedded software CONWEP in LS-DYNA. Conventional Weapons Effects (ConWep) automates the use of the design charts in UFC 3-340-01. It is important to note that the data that ConWep contains is not available to the public. The results showed that when the charges got progressively larger, the damage and overall failure of the tunnels increased. Although the model was able to report that the overall damage increased, due to the simplicity of the model was

not able to account for local failure such as spall and breach. Han et al. stated if they would want to accomplish this task that they would need a much more complicated model.

Single Degree of Freedom Models

To create the initial SDOF model for the thesis we referenced Chapter 5 of structural dynamics textbook by Biggs (1964), which is commonly cited in the blast field. Although we are referencing Biggs, the notation and the thrust of the SDOF explanation is based off of Rodriguez-Nikl (2023). The governing differential equation for a vibrating beam generates an infinite number of degrees of freedom. In a one-degree of freedom system the system's response is approximated by only one mode of vibration. This system for the vibrating beam is seen in Figure 2, which can justify both a standard infinite DOF approach or an SDOF approach.

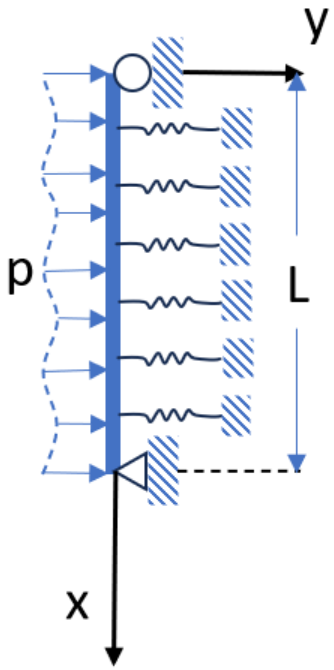

Figure 2: SDOF system with coordinates (p, load x, x-coordinate, L, Length of beam, y, y-coordinate)

This differential equation has an acceleration term, a stiffness term, total resistance, loading term and a damping term which was neglected. The equation of motion for this system is seen in equation 2.

$$p(t) - R(y) = m\ddot{y} \tag{2}$$

where *p* represents the load with respect to time, *R* represents the nonlinear resistance function of the liner, *y* represents the deflection, *m* represents the mass, and ÿ is acceleration.

We will now start deriving the SDOF formulation. The terms for mass, load, and resistance each have an equivalent factor which needs to be calculated. The deflection of the beam can be written as y(x,t) and by using the technique separation of variables it is written as $\phi(x)z(t)$. Where ϕ is a term used to define the shape function, and z is the deflection of the liner at the location where the shape function takes on the value of unity. This new format will be followed throughout the rest of the paper. Moving on, the equation for the equivalent system can be seen in equation 3.

$$\widetilde{M_L}\ddot{z} + \widetilde{R_L} = \tilde{P} \tag{3}$$

Where $\widetilde{M_L}$ represents the equivalent mass, $\tilde{R_L}$ represents the equivalent liner resistance, and $\tilde{P}$ is the equivalent load. To find the equivalent values for mass, load, and resistance we need to introduce certain transformation factors to convert the original system into the equivalent system. These transformation factors, represented by K, vary for the mass, liner resistance and load of the system, each having their own specific value of K. By multiplying these K values with their corresponding factors, they will be converted into

their equivalent values. The equivalent mass for a uniform mass is written by Biggs as equation 4.

$$\widetilde{M}_L = m_L \int_L \phi^2 \, dx \tag{4}$$

This is where m_L is the liner mass in units of Force/Length, and ϕ is the assumed-shape function which depends on whether the deflection of the beam is in an elastic or plastic stage of deformation. This will be discussed more later in the paper. Biggs later writes this equation in terms of the tabulated mass constant K_M, which is expressed by equation 5.

$$\widetilde{M}_L = K_M M_L \tag{5}$$

In this equation, M_L is the total mass of the liner, which is equal to m_L multiplied by the length L or span of the beam. If we set equations 4 and 5 equal to each other we can solve for our K_M value as seen in equation 6.

$$m_L \int_L \phi^2 \, dx = K_M m_L L \tag{6}$$

Therefore, the equation for the uniform mass factor K_M is given to be:

$$K_M = \frac{1}{L} \int_L \phi^2 dx \tag{7}$$

The equivalent load is found in a similar manner. In the case of a uniform load the equivalent load is simplified as seen in equation 8.

$$\tilde{P} = p \int_L \phi \, dx \tag{8}$$

Writing equation 8 in terms of the tabulated load constant K_L yields the expression in equation 9.

$$\tilde{P} = K_L P = K_L pL \tag{9}$$

In this expression, P represents the total load and p represents the applied distributed load in units of Force/ Length. The equivalent load factor K_L in the case of a uniform loading is found to be:

$$K_L = \frac{1}{L}\int_L \phi \, dx \tag{10}$$

Lastly, the expression for the equivalent liner resistance is:

$$\tilde{R}_L = \int_L M''\phi dx \tag{11}$$

Recalling from beam theory, when there is a statically loaded beam, the distributed load applied to the beam with no soil behind it is equal to the second derivation of its bending moment M''. This means if the load causing internal moments is assumed to be equal to "p", then $M'' = p$. Plugging in this assumption into equation 11 yields

$$\tilde{R}_L = \int_L p\phi dx \tag{12}$$

Biggs gives the equivalent resistance in terms of a tabulated resistance constant K_R as is seen in equation 13.

$$\tilde{R}_L = K_R R_L \tag{13}$$

In this equation R_L represents the total resistance of the liner. Following the explanation that $R_L = \int_L M'' dx = \int_L p dx$, substituting this information into equation 13 and setting equations 12 and 13 equal to one another we can solve for K_R. We are assuming that the load is uniform and solving for K_R gets us equation 14.

$$K_R = \frac{1}{L}\int_L \phi \, dx \tag{14}$$

If we compare both the equations 14 and equation 10 we can see that the equivalent liner resistance factor K_R is equal to the load factor K_L.

$$K_R = K_L \tag{15}$$

Moving on from the equivalent transformation factors we need to discuss additional aspect essential for setting up our SDOF model. The resistance of the liner is non-linear. The resistance R_L is computed as a load-deflection curve, also known as a resistance function. This is computed by an analysis of an elastic beam with plastic hinges. Once the plastic hinge is formed two things occur: the shape changes and the resistance of the liner R reaches it maximum value Ru. The shapes can be broken down into the elastic deformation, the yield point, and plastic deformation.

The shape function ϕ is based on the static deflected shape of a beam subjected to a load *p*. For our equivalent system we are considering the segment of the tunnel liner to be represented by a simply supported beam, and the load from the charge to be represented as a distributed load. For a uniform load, the elastic shape function can be seen in equation 16, and the plastic shape function can be seen in equation 17. The reason we require both these sets of equation(s) is because we have non-linear resistance.

$$\phi_e = \frac{16x}{5L^4}(L^3 - 2Lx^2 + x^3) \tag{16}$$

$$\phi_p = \begin{cases} \frac{2x}{L}, & x < \frac{L}{2} \\ 2\left(1 - \frac{x}{L}\right), & x \geq \frac{L}{2} \end{cases} \tag{17}$$

The deflection of the beam is given by equation 18.

$$v = \begin{cases} \phi_e z, & z < z_y \\ \phi_e z_y + \phi_p(z - z_y), & z \geq z_y \end{cases} \tag{18}$$

The first half of equation 18 is used for all equations related to the elastic deflection, while the second half is used for when the plastic deformation is past the yield point. The yield deflection is seen in equation 19.

$$v_y = \phi_e z_y \tag{19}$$

Focusing first on the elastic shape function, the integrals for the equivalent factors evaluate to the following values.

$$K_M = \frac{3968}{7875} = 0.504 \tag{20}$$

$$K_L = \frac{16}{25} = 0.64 \tag{21}$$

These values have also been tabulated by Biggs. For the plastic shape function, for the integrals above evaluate to:

$$K_M = \frac{1}{3} = 0.333 \tag{22}$$

$$K_L = \frac{1}{2} = 0.50 \tag{23}$$

The displacement progression of the tunnel liner changes depending on the deformation stage of the beam. When the beam is first loaded it begins in the elastic deformation

stage. Once a moment at the midspan reaches the moment capacity and a hinge is formed, the subsequent deformation is in a plastic mechanism with a hinge at midspan.

Aside from just the equivalent factors, the tables from Biggs also give us the maximum resistance and stiffness constant for a liner. For a simply supported beam subjected to a distributed uniform load *w* the maximum moment is $\frac{wL^2}{8}$. When the moment reaches the plastic moment capacity of the cross section M_p is how we know that the maximum resistance has been reached. Solving for the maximum load wL yields the following value for the ultimate resistance:

$$R_m = \frac{8M_p}{L} \tag{24}$$

To find the stiffness we need to use the maximum deflection of a simply supported beam which is $5wL^4/384EI$. Stiffness is equivalent to the load wL divided by the deflection, giving us the following value:

$$k = \frac{384EI}{5L^3} \tag{25}$$

We have obtained all the required variables to solve for our single degree of freedom system, the response must now be computed numerically. Biggs defines the following approach, which was adopted for this study. The initial acceleration for the first-time step is found by using the equation 26, which is found by rearranging the governing equation (equation 2).

$$\ddot{z}(1) = \frac{(KL \cdot p \cdot L)}{\widetilde{M}_L} \tag{26}$$

The accelerations in subsequent time steps are found using equation 27.

$$\ddot{z}(t) = \frac{(KL \cdot p \cdot L - KL \cdot R_L)}{\widetilde{M}_L} \tag{27}$$

The variable R_L represents the liner resistance. Where z represents the displacement of the liner to solve for the initial displacement, we use equation 28.

$$z^{(1)} = \frac{1}{2} z^{(0)} (\Delta t)^2 \tag{28}$$

The subsequent deflections are measured using the following equation.

$$z^{(i)} = 2z^{(i-1)} - z^{(i-2)} + \ddot{z}^{(i-1)} (\Delta t)^2 \tag{29}$$

The notation z represents our displacement at a specific time, what $z^{(i-1)}$ represents is the displacement value at the previous time station and so on. This notation works for both displacement and acceleration. The reason we need equation 28 to set up the initial displacement value is because equation 29 requires displacement values from two previous time steps. These equations were used to find the final displacement of the tunnel liner without soil.

The computation of reactions and internal forces can be accomplished with SDOF methods but that is outside the scope of this thesis. Now that the initial idea of the theory is set up, the next step is explaining the addition of soil and the new variables we had to implement.

CHAPTER 2

Explanation of Update to Theory

In the last chapter we discussed how the derivation of a SDOF model with no soil. This is different from our scenario because we are considering the soil behind the liner. For the soil we must consider its two major components that would affect the maximum displacement, the soil's mass and the soil's resistance. The extension of the SDOF model comes from Rodriguez-Nikl (2023).

The governing equation we used previously seen in equation 2 changes when we add soil to the system as seen in equation 30:

$$p(t) - R(y) - f_s = m\ddot{y} \tag{30}$$

In this equation f_s represent the resistance of the soil in units of Force/Length. The equivalent single degree of freedom differential equation with soil can be seen in equation 31.

$$(\widetilde{M}_L + \widetilde{M}_s)\ddot{z} + \tilde{R}_L + \tilde{R}_S = \tilde{P} \tag{31}$$

Where $\widetilde{M}_s$ is the term for equivalent soil mass. The term $\tilde{R}_S$ represents the equivalent soil resistance.

The following topics will cover what changes happen to the system when soil is added. We first need to find the equivalent mass of the soil. Equivalent mass of the soil is given by equation 32.

$$\widetilde{M}_s = \frac{m_s}{2}\int_L \phi^2 dx \tag{32}$$

In this equation m_s is the mass of the soil in units of Force/Length, and ϕ^2 is related to the shape function of the system. Rodriguez-Nikl proposed as a hypothesis that the inertial force for the soil only uses one half of the soil mass because it is assumed that one end of the soil blocks moves from the liner while the other end at a yet unspecified depth d_e away does not move. This term d_e will be used as a tuning parameter in the model, and will be assumed to be constant through subsequent calculations. Hence, this explains why we see in both equations 32 and 33 are divided by 2. Equation 33 is another form of writing the equivalent mass of soil terms of the transformation factor K.

$$\widetilde{M}_s = K_M \frac{M_s}{2} \tag{33}$$

K_M is the equivalent mass transformation constant that was explained in chapter 1. The term M_S is the total mass of the soil. Next, we will talk about the equivalent soil resistance which is shown in equation 34.

$$\tilde{R}_s = \int_L f_s \phi dx \tag{34}$$

In this equation f_s is the resistance for a distributed elastic foundation. The resistance can be written in terms of soil stiffness and the liner deflection, which is shown in equation 35:

$$f_s = k_s v \tag{35}$$

The soil stiffness was computed from the expression proposed by Vesic (1963, eq 24) for a beam resting on a semi-infinite elastic foundation:

$$k_s = 0.65 \sqrt[12]{\frac{\alpha E_s B^4}{EI}} * \frac{\alpha E_s}{1 - v_s^2} \tag{36}$$

The semi-infinite elastic foundation in this case is the soil behind the tunnel liner. This stiffness is assumed to be constant over the length of the beam. The notation in Equation 36 has been modified slightly from its original appearance in this report keep consistent with the report written by Rodriguez-Nikl. The term B is defined by Vesic as the width of the beam. Presented herein is the first obstacle we encountered. In the present problem there is a continuous liner with no clear edge (as would be the case with a foundation). Thus, it is not clear what value that should be used for B. Therefore, we will be using B as a fitting parameter for our model. The term α represents a reduction factor to the modulus to account for soil nonlinearity. This nonlinearity is said to come from two separate sources. The first is the nonlinear behavior of the soil and the second is the non-uniform compression of the soil. The soil near the midspan will compress considerably more than the soil near the supports. As stated, by Rodriguez-Nikl, lumping both sources of linearity together with a secant modulus is an oversimplification, but the question at this stage is whether this method works. We are trying to get acceptable prediction using reasonable values of α, B, and effective depth d_e .

To initialize the derivation, equations 34 and 35 are combined. While also recognizing that k_s is a constant, after combing the equation, we get equation 37.

$$\tilde{R}_s = k_s \int_L v\phi dx \tag{37}$$

In this equation $\tilde{R}_s$ is the term for the equivalent soil resistance. This equation is applied to both the pre- and post-yield stages. To determine the equivalent soil resistance before the liner yields, we must substitute the first part of equation 18. By doing so the equivalent soil resistance for the elastic portion of the deflection is obtained as seen in equation 38.

$$\tilde{R}_s = \left[k_s \int_L \phi_e^2 \, dx \right] z \tag{38}$$

The term z represents the deflection of the system. It is similar to the y value we spoke about in chapter 1. Equation 38 represents the equivalent soil resistance, which depends on the equivalent soil stiffness in square brackets which is repeated in equation 39.

$$\tilde{k}_{se} = k_s \int_L \phi_e^2 \, dx \tag{39}$$

The equivalent soil spring stiffness changes after it yields and begins post-yield deformation. For us to determine the equivalent soil resistance after the liner yields, we must incorporate the second half of Equation 18 and plug that into equation 37, doing so we obtain equation 40.

$$\tilde{R}_s = k_s \int_L \left[\phi_e z_y + \phi_p (z - z_y) \right] \phi_p dx \tag{40}$$

This equation can be simplified into equation 41.

$$\tilde{R}_s = k_s \int_L \phi_e \phi_p dx \, z_y + k_s \int_L \phi_p^2 dx (z - z_y) \tag{41}$$

From equation 41 we can pull that the equivalent soil resistance immediately after soil yields is equation 42.

$$\tilde{R}_{spy} = k_s \int_L \phi_e \phi_p dx \, z_y \tag{42}$$

The equivalent soil stiffness during plastic liner behavior is seen in equation 43.

$$\tilde{k}_{sp} = k_s \int_L \phi_p^2 \, dx \tag{43}$$

Since equation 39 and 43 are similar, the following equation can be written for the equivalent soil stiffness with the understanding that the appropriate shape function should be used:

$$\tilde{k}_s = k_s \int_L \phi^2 \, dx \tag{44}$$

The liner resistance also has an update when soil is added. Recalling from chapter 1, when there is a statically loaded beam, the distributed load was applied to the beam with no soil behind it meaning it was equal to the second deviation of its bending moment M''. This meant that if the load causing internal moments is assumed to be equal to "p", then M'' = p. This is different from what we required now because we are looking at a statically loaded beam on an elastic foundation, meaning the assumption from before is not adequate. Therefore, it is assumed that the second derivation of the bending moment in the soil-supported beam is proportional to the applied load. Which is basically stating $M'' = p - f_s \approx ap$, where "a" represents a proportionality constant which will canceled out from subsequent calculations. Although this assumption was relaxed the outcome did not change. The equivalent liner resistance factor K_R was still equal to the load factor K_L.

After the initial step of obtaining the equivalent factors for both the mass and stiffness of the soil, we can move onto solving for our required values.

The pre-yield equation for the equivalent soil stiffness during the elastic liner behavior is written as follows:

$$\tilde{k}_{se} = \frac{3968 k_s L}{7875} = 0.504 k_s L \tag{45}$$

The post-yield equations for the equivalent soil stiffness during the plastic liner behavior is seen in equation 46.

$$\tilde{k}_{sp} = \frac{k_s L}{3} = 0.333 k_s L \tag{46}$$

The soil resistance immediately after the liner yields is defined as

$$\tilde{R}_{spy} = \frac{61 k_s L z_y}{150} = 0.407 k_s L z_y \tag{47}$$

As mentioned earlier, we will express the deflection in terms of z which represents the position of the beam in its deflection. The term z_y represents is the value of the deflection where the liner has reached the yield point. Any value of z below z_y is telling us that the deflection of the beam is still in the plastic stage. Once it passes the value of z_y we know we are in the plastic zone of the beam deflection.

Now that the explanation of how the soil will react in with the system, we can now update the numerical calculation used in the program. By rearranging the governing equation seen in equation 2 we can obtain the acceleration at any time step seen in the following equation:

$$\ddot{y} = \frac{K_L p(t_i) L - \tilde{R}_L(z_i) - \tilde{R}_s(z_i)}{K_M[\widetilde{M}_L + 0.5\widetilde{M}_s]} \tag{48}$$

The liner resistance for both the elastic and plastic shape functions are as follows:

$$\widetilde{R_L}(z_i) = \begin{cases} K_L k_L z_i & z < z_y \\ K_L R_u & z \geq z_y \end{cases} \tag{49}$$

The soil resistance can be written as the following:

$$\widetilde{R_s}(z_i) = \begin{cases} \tilde{k}_{se} z_i & z < z_y \\ \tilde{R}_{spy} + \tilde{k}_{sp}(z_i - z_y) & z \geq z_y \end{cases} \tag{50}$$

The first half of equations 49 and 50 are meant to be used for the elastic portion and the second half is to be used for plastic portion of beam deflection. With the addition of soil accounted for we can now begin testing our model.

CHAPTER 3

Verification of computational model

Verification Without Soil

With any numerical model running checks is necessary to test the accuracy. For this model three checks were conducted. These checks were done to ensure that the liner behavior without soils present gave proper values that matched up with theoretical results. The checks were based on examples found in the Biggs textbook. To exclude the consideration of soil, we set the values of soil mass m_S and Young's modulus E_S to zero. The system will be excited by setting up pressure time history that follows the textbook examples.

Period Check

The first of these checks was to compare the period determined by the numerical model to the theoretical period, which is given by

$$T = 2 \cdot \pi \cdot \sqrt{M/K} \tag{51}$$

The method in which we determined the numerical model period is by measuring the elapsed time between displacement peaks in the numerical model. The excitation used for the period is the free vibration after a forcing function we used in the third check of the model. The notation T represents period, M represents the equivalent mass of the liner, and K is the equivalent liner stiffness. The value of the mass we used 1.129 lbm and the stiffness was equal to $7.68 \cdot 10^4 \frac{\text{lb}}{\text{in}}$. The period according to Equation 51 was 0.0258 seconds, while the period based on the numerical simulation was 0.0257 seconds. The period is accurate enough for us to feel comfortable with continuing to use this model.

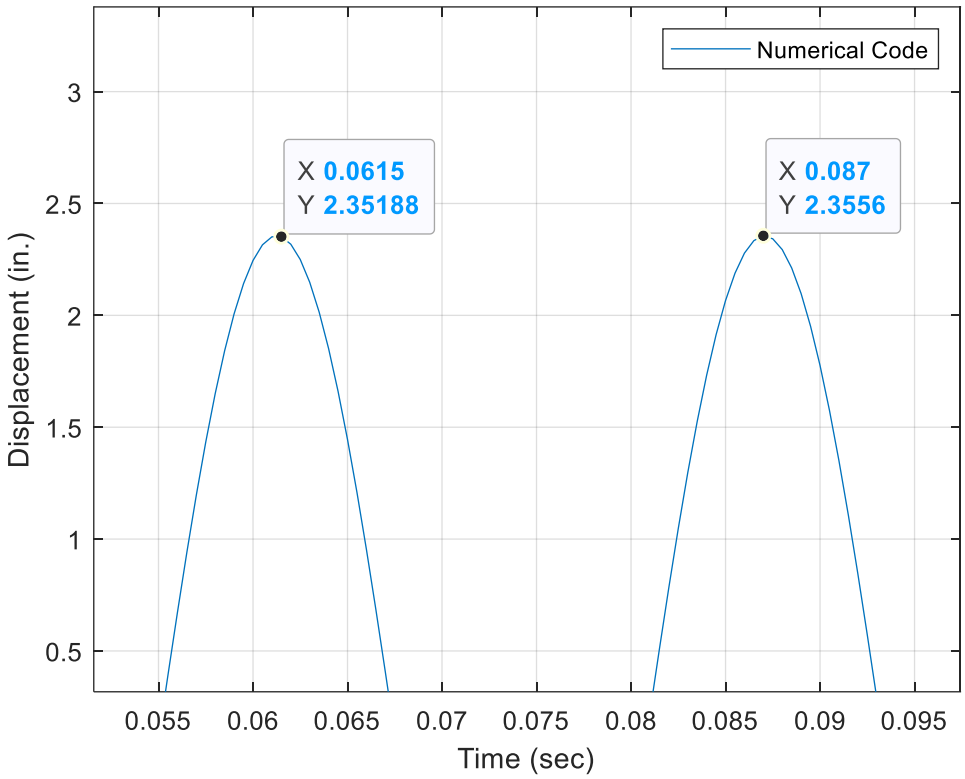

Figure 3:Displacement vs. time period check.

Uniform deflection check

The next check conducted was for the deflection under quasi-static uniform loading. The output from the model should be equal to the following equation:

$$\Delta = \frac{5wL^4}{384EI} \tag{52}$$

where Δ is the symbol used for deflection, w represents the uniform load, L is the length of the beam, E is equal to the Young's Modulus, and I represents the moment of inertia. To apply the quasi-static loading in a model designed for dynamic loading, the load duration was made very large with a value of 999 seconds, effectively simulating a static problem. The load duration was required to simulate a large duration and not provided by

the example we were following. The value for L was 120 inches, the value of w was $1.667 \cdot 10^3 \frac{\text{lb}}{\text{in}}$, the value of E was $3.60 \cdot 10^6 \frac{\text{lb}}{\text{in}^2}$, and lastly the value for I was $749\ \text{in}^4$. After this alteration to the loading, our value for maximum deflection was very close to the value of the quasi-static beam loading. The maximum deflection value obtained from equation 52 was 1.6658 inches and the value from the model was 1.6669 inches. The values of the deflection that came from the model matched almost identically to the value from equation 52, that we felt it was appropriate to continue to the third and final check.

Forcing function check

The last check performed to prove the model's accuracy was to compute the response to a known forcing function. A rectangular forcing function was used as described in Biggs (1964). What we are comparing is the numerically computed displacement with the displacement given by equations 2.10 and 2.16a in Biggs, which govern the deflection of a single degree of freedom system subjected to a square pulse. Equation 2.10 is the response during the pulse and 2.16a is the response after the pulse ends. Equation 2.10 is reproduced in equation 53 and Equation 2.16a is seen in equation 54.

$$y = \left(\frac{F_1}{k}\right) \cdot (1 - \cos(\omega \cdot t)) \tag{53}$$

$$y = \left(\frac{F_1}{k}\right) \cdot (\cos((\omega) \cdot (t - t_d)) - \cos(\omega \cdot t)) \tag{54}$$

For both equations the y represents the displacement, F_1 represents the constant force value, k represents the spring constant, ω is the term used for the natural frequency, and t represents time. The value of F_1 was $1666.7\frac{\text{lb}}{\text{in}}$ and the value of ω was $243.5\frac{1}{\text{s}}$. Figure 4 shows both the computed displacement using our model and theoretical displacement from Biggs. The displacement calculated by the model and the displacement calculated using the equations from Biggs overlap and give the same deflection values. With these checks completed we can now feel comfort in knowing that the numerical model involving only the liner is accurate enough to use for the next phase of the project.

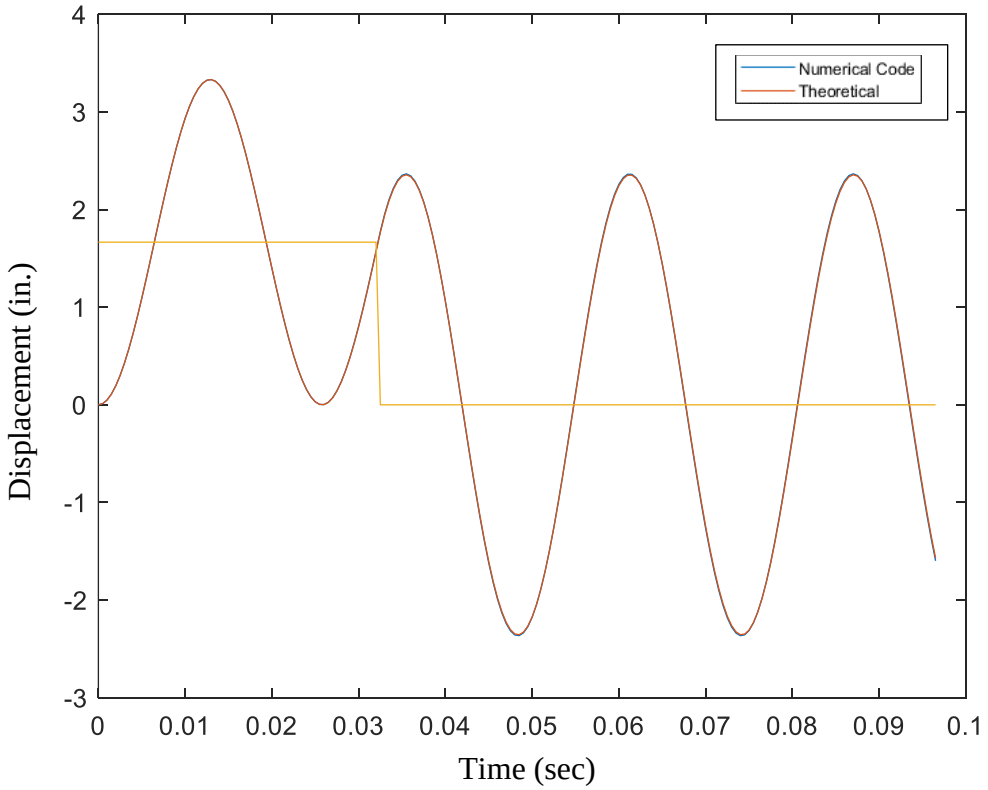

Figure 4: Theoretical and computed displacement place on top of one another. Yellow line is the static deflection.

Verification With Soil

The second verification of the model came from comparing our deflection with the results of Goel et al. (2021). The reason behind choosing this study is because it used a model that accounted for soil surrounding the tunnel liner and provided all of the input variables necessary to replicate their results with our model. As stated in Ch. 1, Goel et al. performed a finite element (FE) analysis of a shallow tunnel experiencing a blast inside the tunnel, with soil as its surrounding medium and a structure on the ground level. The FE analysis tool they used to simulate the blast loading was ABAQUS/Explicit. Their main goal was to focus on the damage the superstructure underwent with the change in tunnel cross sectional shape while keeping all other factors constant. Despite their main goal differing from our own they did provide the relevant displacement history for the tunnel liner. There were three tunnel shapes which were considered in their analysis circular, rectangular, and horseshoe. For our purposes we will be looking specifically at their results for the rectangular tunnel.

With the properties available, we could successfully replicate their study. The following tables show both the values obtained from the paper and the values calculated by us shown in bold that relate the table. Because our model used English units there were many conversions that needed to occur to be able to use the data provided. Table 1 lists the global dimensions of the tunnel. Table 2 provides the cross-section properties of the liner. Table 3 provides the value of Young's modulus of the material. Table 4 provides the density of the material. Table 5 provides contains the yield strength of the

material. Table 6 provides the weight of the charge and the max deflection of the tunnel liner.

Table 1: Global dimensions of the tunnel

Dimensions of tunnel	Meters (m)	Inches (in)
length	20	787.402
Width	5.4	212.598
Height	4.241	166.974

Table 2: Cross-section properties of the liner

Liner Dimensions	Meters (m)	Inches (in)
Height	0.3	11.811
Width	0.3	11.811
Steel Reinforcement Dia.	0.01	0.394
Area of Steel Reinforcement		0.122 in^2

Table 3: Youngs Modulus of the materials

Material	Youngs modulus, E/GPa	Youngs modulus, E/(ksi)
RC lining	35.35	5127.084
Steel Reinforcements	200	29007.548
Soil	0.025 or 25 MPa	3.626

Table 4: Density of the materials

Material	Density, kg/m^3	Density, lbm/ft^3
RC lining	2400	149.827
Soil	1560	93.388

Table 5: Yield Strength of the material

Material	Yield Strength, MPa	Yield Strength, psi
RC lining (M50)	50	7251.887
Steel Reinforcements (Fe415)	415	60.191

Table 6: Weight of the charge & Max deflection of the tunnel liner

Weight of Charge	100 kg	220.462 lbm
Deflection	29.16 mm	1.148 in.

The first of the many calculations needed to obtain all the information needed to use this report started with finding out the height of the rectangular tunnel. Goel et al. stated that for all tunnel shapes the widths were all 5.4 meters and each the cross-sectional areas were equal. To find the height for the rectangular tunnel we used the area of the circular tunnel. The process of find the rectangular tunnels height is shown is equations 55 and 56.

$$A_T = \frac{\pi * W^2}{4} = 22.902\ m^2 \tag{55}$$

$$H_T = \frac{A_T}{W_T} = \frac{22.902\ m^2}{5.4m} = 4.241\ m = 166.974\ in \tag{56}$$

Goel et al. did not provide the pressure time history. The use of design manual UFC 03-340-02 was used to find the pressure time history. The reason we aren't using software like ConWep, as we mentioned in chapter 1, is that it is not available to be used by the public. What this meant is that our next best option was to use the UFC 03-340-02 manual.

Prior to utilizing the design manual for determining the pressure time history, we approximated our tunnel as a very tall sideways cubicle. After doing so we followed the steps laid out by the design manual. The first step in this process is to use Figure 2-51 of the UFC 3-340-02, which is titled "Barrier and cubicle configurations and parameters". This figure displayed multiple configurations of cubicles. For our tunnel we chose a four-wall cubicle with roof. The four walls of the cubicle thus represent the walls, bottom and top of the tunnel. The floor and roof of the cubicle represent the open ends of the tunnel. Representing them as a solid floor and roof essentially states that the tunnel does not vent rapidly. Figure 5 shows the tunnel cubicle geometry.

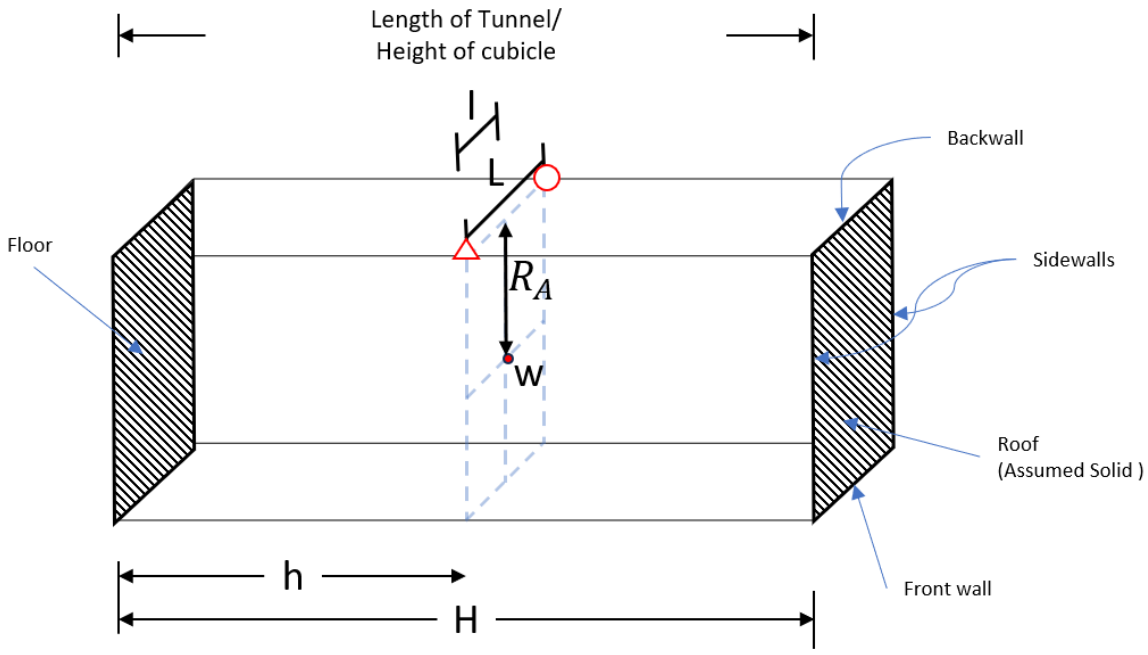

Figure 5: Tunnel cubicle geometry

After referring to Figure 5 and utilizing the values obtained from the previous tables, we have all the necessary components required to find the pressure time history. These parameters include $N, \frac{l}{L}, \frac{h}{H}, \frac{L}{H}, \frac{L}{Ra}, Za = \frac{Ra}{w^{1/3}}$. In this context, $R_a$represents the standoff distance to the relevant surface. The dimension L represents the width of the tunnel, whereas lower case l is the perpendicular distance from the adjoining element to the charge. The reason why l is equal to half of L is due to the charge being positioned at the center of the tunnel width. Similarly, H represents the length of the tunnel, which we have assumed to be near infinite, and lower-case h like l is equal to half of H because the charge is placed at the center of the tunnel. Lastly, N represents the number of reflecting surfaces adjacent to the surface in question, which, according to our cubicle arrangement, is set at 4.

In the following, the computed values are detailed for the necessary parameters. The distance R_a is half of the height of the tunnel liner, which we calculated for previously.

$$Ra = \frac{4.24m}{2} * \frac{3.2807\ ft}{1\ m} = 6.89\ ft = 83.46\ in. \tag{57}$$

We use the value of 212.6 inches for L (the width of the tunnel).

$$L = 212.6\ in \tag{58}$$

The number of reflecting surfaces is 4:

$$N = 4 \tag{59}$$

In both cases for l/L and h/H, both are equal to 0.5 because we placed our charge in the center most point in the tunnel.

$$\frac{l}{L} = 0.50 \tag{60}$$

$$\frac{h}{H} = 0.50 \tag{61}$$

The reason why we get zero for L/H is because we are assuming H to be very large. The smallest tabulated value for L/H is 0. 625. This value was used in subsequent calculations.

$$\frac{L}{H} \rightarrow 0, use\ 0.625 \tag{62}$$

Based on the values of L and Ra computed above

$$\frac{L}{Ra} = 2.547 \tag{63}$$

The last parameter to be calculated is the scaled distance:

$$z = \frac{Ra}{w^{\frac{1}{3}}} = \frac{6.89\ ft}{220.4\ lb^{\frac{1}{3}}} = 1.140(\frac{ft}{lb^{\frac{1}{3}}}) \tag{64}$$

Pressure and impulse were found using figures in the UFC 03-340-2 manual each with their own set of graphs. The appropriate figure was selected to match the values of N, I/L, and h/H. Each graph on the figure had a different L/H value, and as was previously stated, the smallest possible value was used because there were no zero valued graphs. We used the following graph from Fig. 2-100 seen in Figure 6 to find our pressure given in psi.

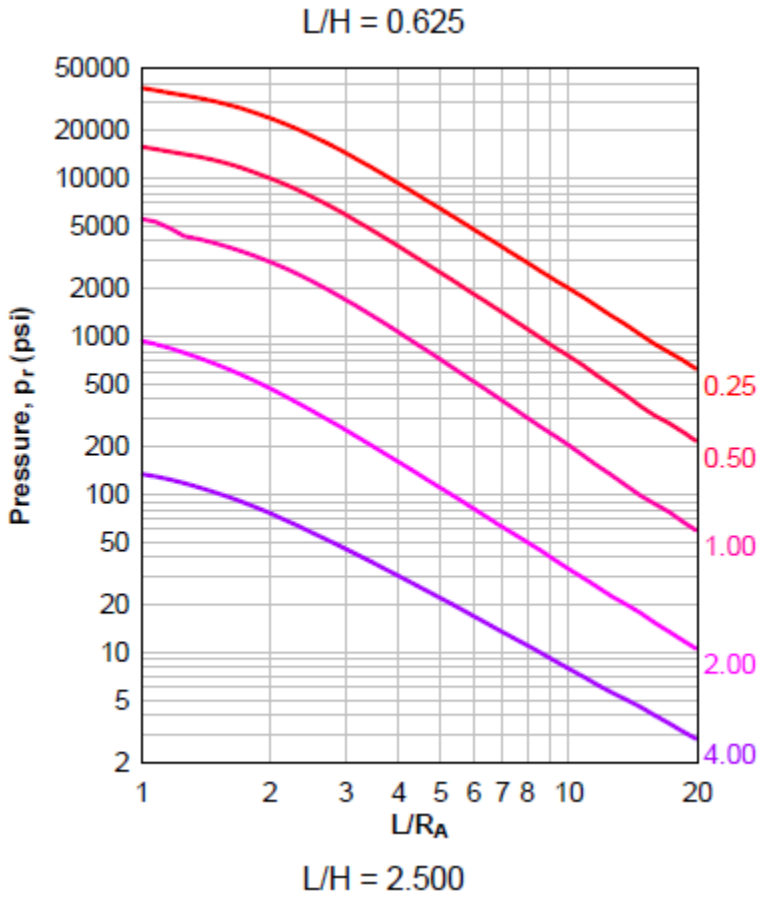

Figure 6: Department of Defense, 2008, Figure 2-100 (N=4, l/L=0.50, h/H=0,50)

We used the following graph from, Fig. 2-149 seen in Figure 7 and was used to find our impulse. Although this figure provides results in units of psi-ms/lb$^{1/3}$, this can be solved for impulse in psi-ms.

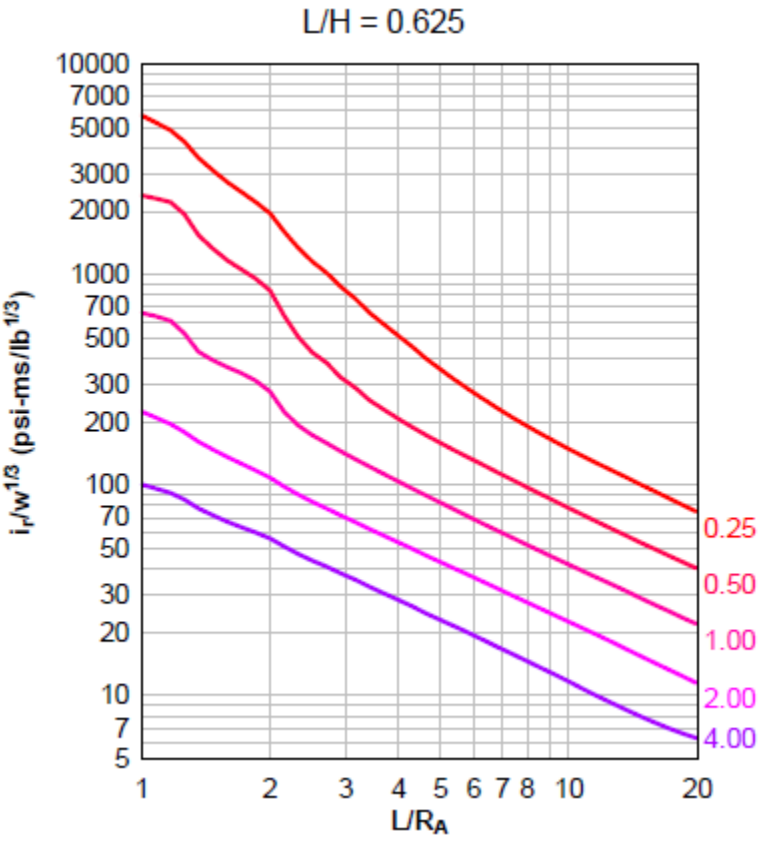

Figure 7: Department of Defense, 2008, Figure 2-149 (N=4, l/L=0.50, h/H=0,50)

For the scaled distance, the figures in UFC used whole numbers, which meant interpolation had to be used to get the right pressure and impulse values. The value obtained for pressure was 1525.9 psi, and the value obtained for impulse was 894.83 psi-ms. To find time we can use Figure 8 which shows the relationship between pressure, impulse and time. Impulse is equal to the area of the pressure time history, the equation

for impulse can be seen in equation 65.

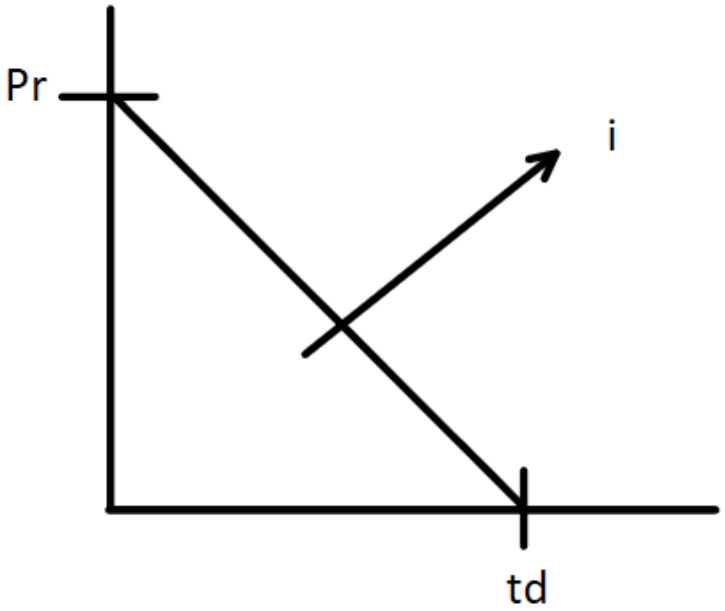

Figure 8: Inverse triangular pressure time history

To solve for time, we take equation 65 and solve for t, this solution can be seen in equation 66 and in Fig. 8.

$$i = \frac{p_r t_d}{2} \tag{65}$$

$$t_d = \frac{2i}{p_r} = 1.1728\, ms \tag{66}$$

With the time now calculated the pressure time history is fully defined.

The last few properties we needed were the plastic moment M_p and the EI of the reinforced concrete given the cross-sectional information. In order to obtain these values,

we used a cross-sectional analysis program called Response 2000. This program allowed us to specify a reinforced concrete segment to compute the cross-sectional properties from the geometrical and material definitions. Figure 9 shows the reinforced concrete segment that was designed in the program. Goel et al. used 10 mm steel bars which we equated to #3 steel bars and we assumed a 3-inch cover on both sides.

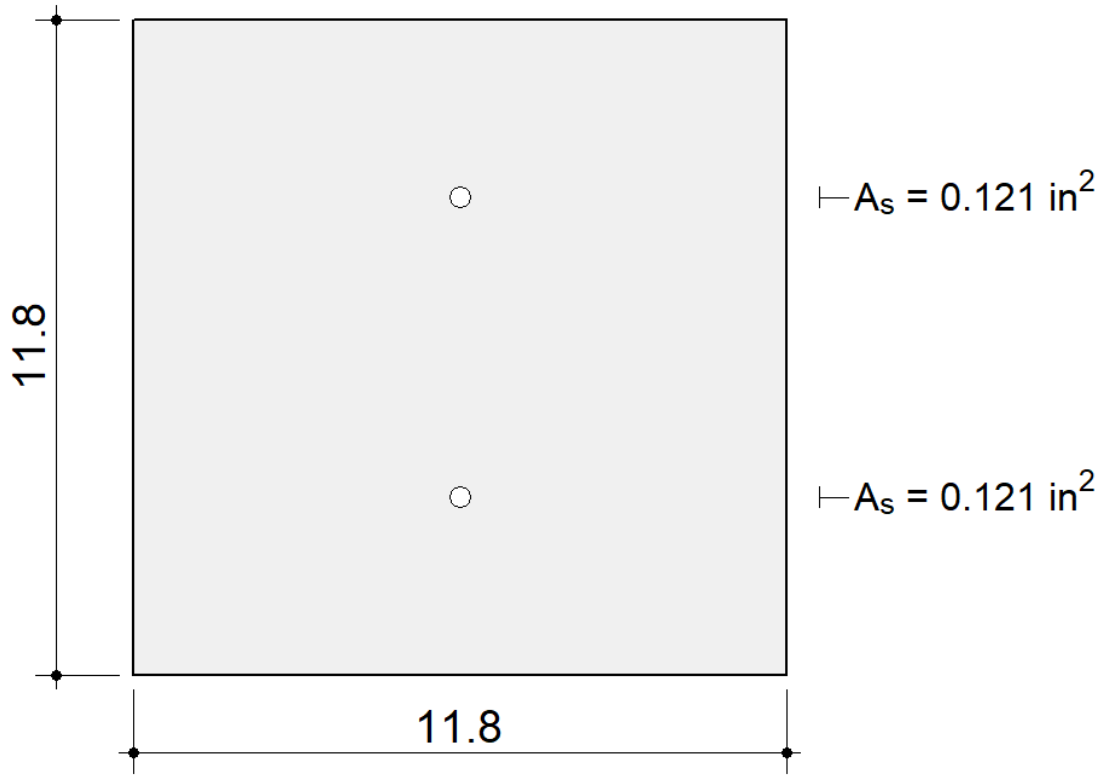

Figure 9: Response 2000 reinforce concrete cross sectional view

Response 2000 calculated the moment curvature curve for the cross section. Figure 11 shows the moment-curvature curve obtained from Response 2000 and a bilinear fit. The bilinear curve depended on the expected maximum curvature. To obtain it, we used ideas and mathematics seen in Figure 10. Figure 10 illustrates that the deflection Δ is related to

the rotation θ through geometry. The relation between the two can be seen in the $\tan\theta = \frac{\Delta}{L/2}$ equation seen in Figure 10. Rotation is the integral of the curvature. Assuming a plastic hinge with constant curvature in the hinge, the rotation 2θ (shown in Figure 10) is the length of the plastic hinge Lp times the curvature ϕ. Given a value for Δ of 1.2 inches (from Goel et al.) and a plastic hinge length was assumed to be the same length as the depth of the member (12 inches), we can solve for the maximum of 0.00189 radians/inch.

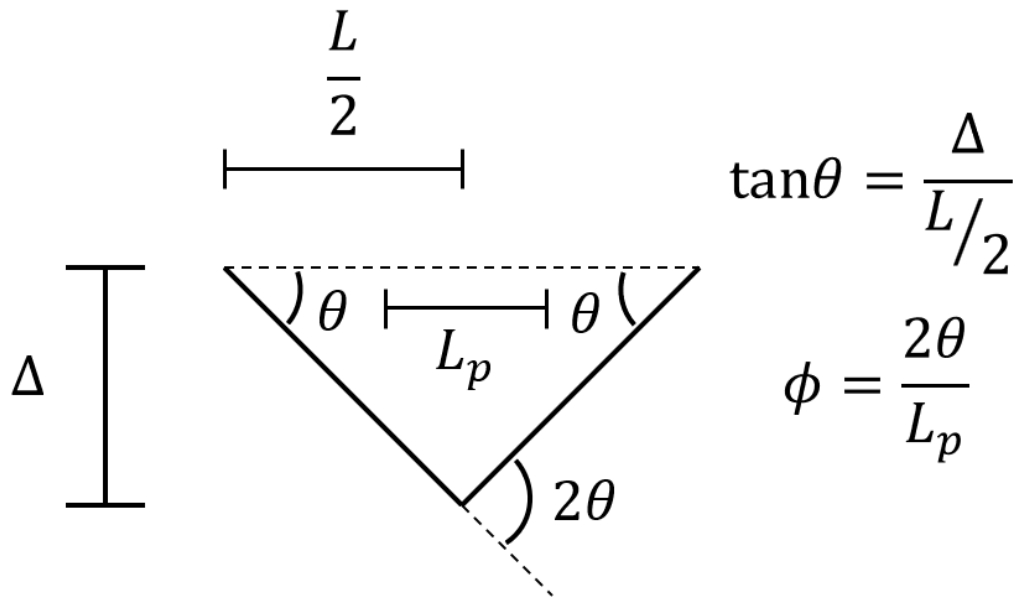

Figure 10: Expected curvature mathematics

In Figure 11 the initial peak seen in the moment curve is ignored because it is assumed that once the liner is subjected to the blast, the liner will have cracked in service and no longer be able to develop that peak moment. The values of the bilinear line were found iteratively so that the area under the black curve was the same as the area under the red curve. The slope of the initial part of the bilinear curve is EI. We used the value of the slope to get the moment of inertia I given that the value of E is known.

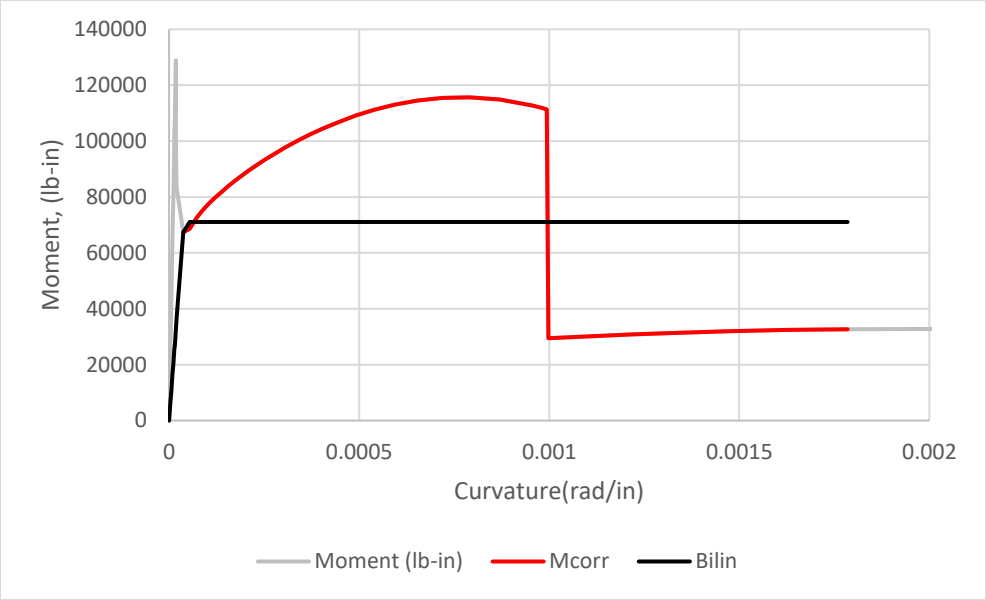

Figure 11:Response 2000 curve and the Bilinear Curve

The resulting values are summarized in Table 7.

Table 7: Response 2000 output values

Response 2000	Values & units
Mp, plastic moment	71066 kip*in
I, moment of inertia	375 in^4

After the final missing parameters we obtained, all values were plugged into the model. The max displacement for the rectangular tunnel shape in Goel et al. model was 29.16 mm or about 1.15 inches. In order to get close to this value we needed to use our models tuning parameters B, α, and d_e. The values we used for our tuning parameters are seen in table 8.

Table 8: Tuning Parameter Values used to math Goel et al. deflection

B	212 inches
α	0.8 unitless
d_e	3 inches

With these tuning parameter values we were able to come close to the value from Goel et al. at 1.15 inches in deflection. Figure 12 shows the peak deflection of the model, and the deflection obtained by Goel et al. The results show that the model is able to attain the correct deflection. However, the deflections occur at different times, indicating that additional work is necessary to better match the results.

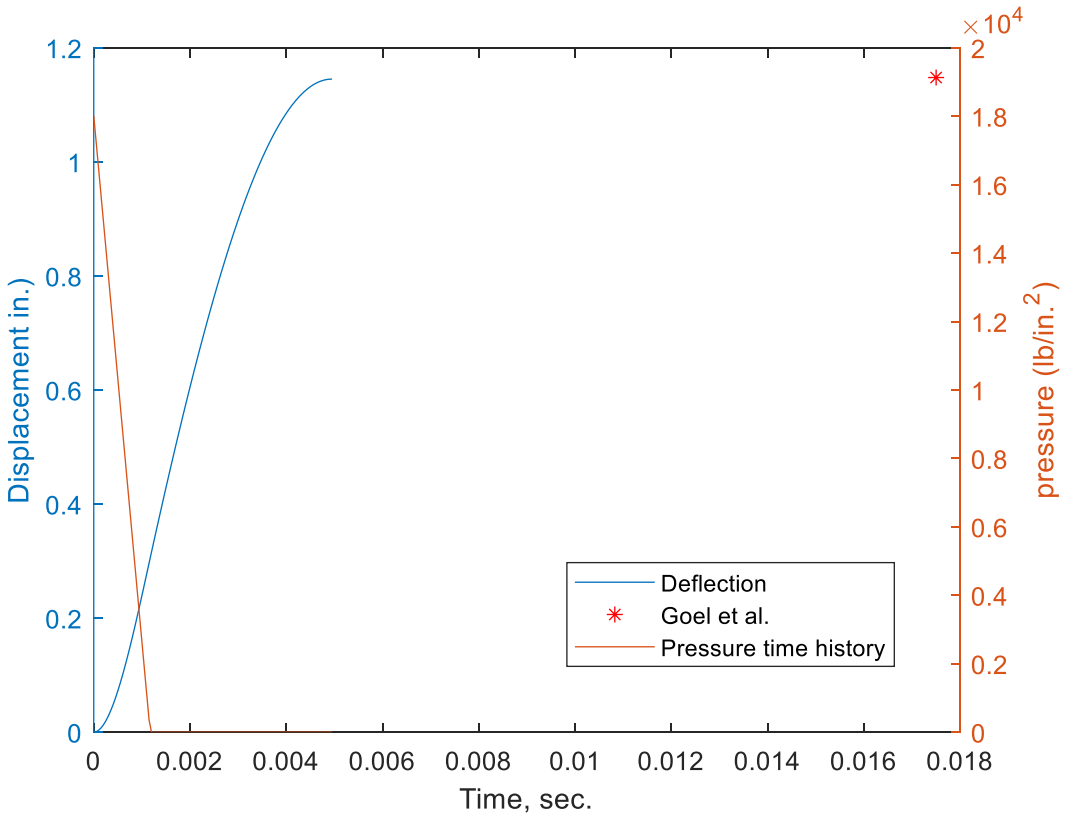

Figure 12: Graphed model deflection with the peak value from Goel et al. and the pressure time history

CHAPTER 4

Discussion and Conclusion

Parameter Variation

In the previous chapter we used three tuning parameters to calibrate the model to obtain an deflection close to what Goel and colleges obtained. Those parameters were the width of the beam B, reduction factor α, and effective depth d_e. The following three figures demonstrate the influence of each parameter on the deflection of the beam. While keeping all other factors constant at the values listed in Table 8, each parameter was tested with varying values to assess its effect.

Figure 13 shows that with the increase of the parameter d_e the deflection decreases. This occurs because while d_e approaches zero, mass of the soil is decreasing, causing there to be less resistance. Variation in this parameter had an almost linear relation to the deflection.

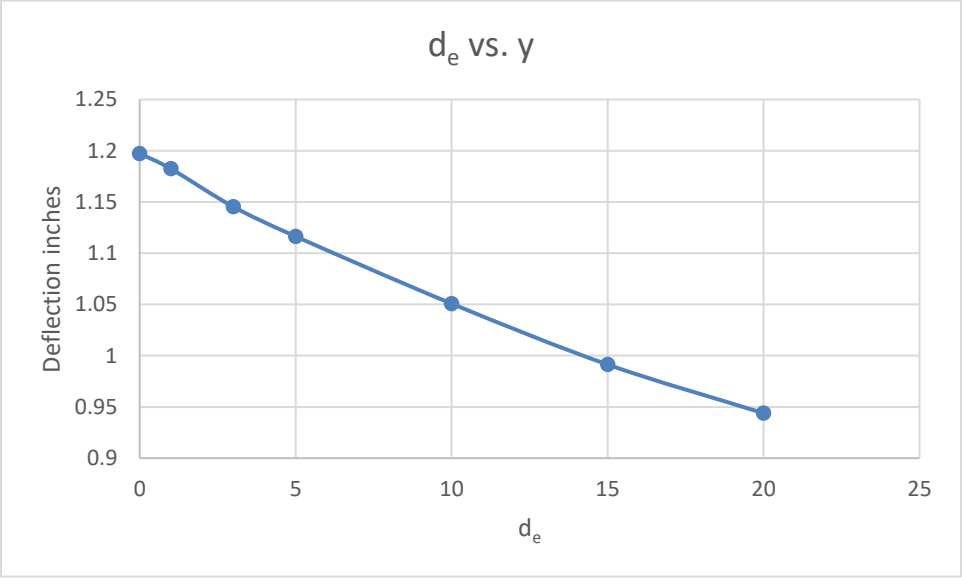

Figure 13: The effect of tunning parameter d_e on the deflection

Figure 14 shows that with the increase of B the deflection decreases. Upon examining Vesic's equation (equation 36), a larger B results in a higher stiffness, which explains the smaller deflection. This occurs due to a smaller beam having more free soil on either side, causing it to be less constrained, therefore less stiff. One more observation to mention is that the relation is linear near the converged value of 212, but the deflection grow faster as B approaches zero.

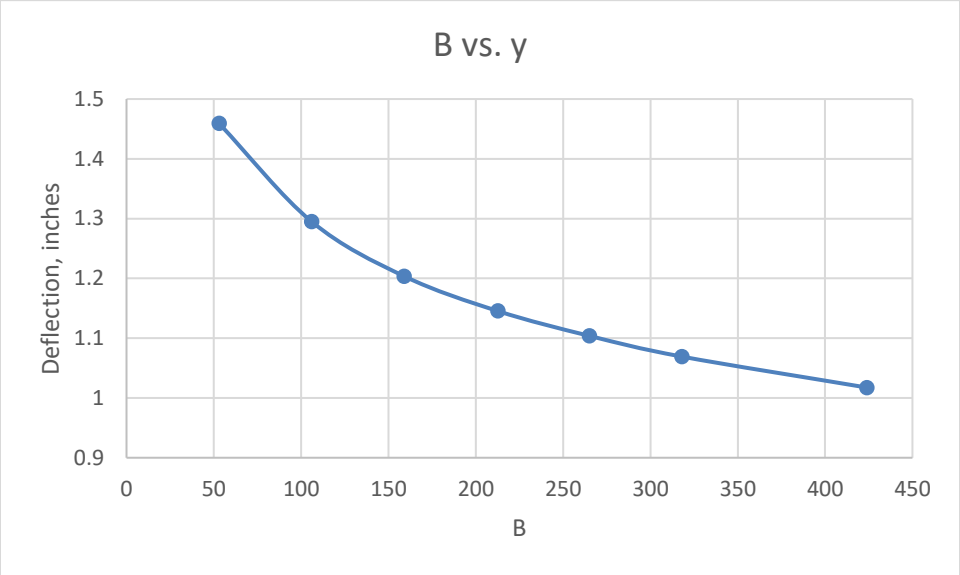

Figure 14:The effect of tunning parameter B on the deflection

Figure 15 shows that with the increase of α, the deflection decreases. As α decreases, so does soil stiffness, which results in lower soil resistance. Near the converged value of $\alpha = 0.8$. the relation between α and deflection is linear and small. However, as α approaches zero, the size of deflection blows up because the liner approaches unrestrained deflection.

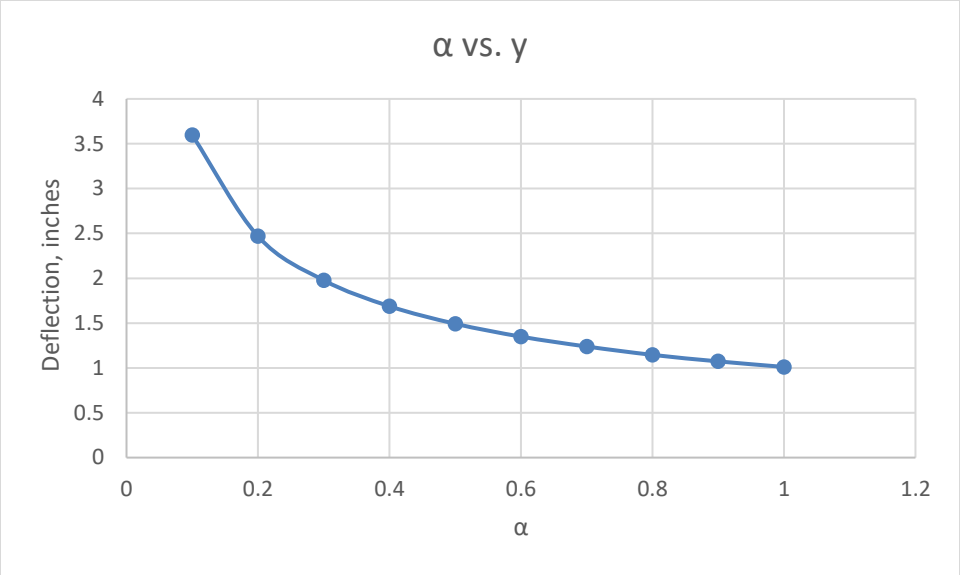

Figure 15: The effect of tunning parameter α on the deflection

Concluding the discussion on the influence of each parameter on the beam's deflection, our focus now shifts to identifying the parameter to which the model is most sensitive. Initially, we will determine the slope in the vicinity of the parameter's converged value and subsequently assess the alteration in deflection resulting from a 10 percent parameter change. This approach is adopted to ensure comparability not solely through slope comparison, but also by introducing a constant derived from the 10 percent change. For d_e, deviating 10 percent from the value of 3 corresponds to a deflection change of 0.0048 inches. In the case of parameter B, a 10 percent deviation from 212 inches results in an averaged deflection change of 0.0199 inches. Lastly, for parameter α, a 10 percent shift from 0.8 yields a deflection change of 0.0675. These values reveal that α exerts the most substantial influence on deflection, followed by B, with d_e having the least significant impact.

Assumptions and Limitations

Many assumptions and limitations related to this research originate from the report written by Rodriguez-Nikl, where he summarized general, liner, load, and soil limitations.

To begin the discussion of limitations and assumptions, we will start off by looking into general issues. To keep consistent with the standard single degree of freedom approach without soil, an assumption was made that the shape function was proportional to the static displaced shape of the beam. Upon adding the soil, the question is whether or not the statement about the shape function still holds true. Further investigation is required to determine the accuracy of the assumption. An additional assumption was made regarding the support conditions for the simplified tunnel liner. For this project we assumed that the liner segment was represented by a simply supported beam, but this could have easily not been the case. It could have been assumed that the liner elements that connect to one another provided significant resistance to rotation. This means that the support conditions may be more accurately depicted as a a fixed-fixed configuration. It is important to note that different boundary conditions can be considered, however with it would come different shape functions and resistances functions. A force we did not consider in the model was damping. Damping for this project was neglected because it was not necessary to complete the objective of peak deflection. This is due to the peak deflection occurring during the first quarter cycle of the response, in which damping can be said to be negligible. Lastly, due to the simplicity of the model we could not measure local failures like spall or breach.

The next set of limitations pertain to the liner. The first assumption for the liner was that the internal forces were proportional to the applied load. This assumption is appropriate when there is no soil behind the liner. However, it is not clear whether the made assumption is sufficiently accurate due to the addition of soil changing the distribution of internal forces. Second, the behavior of the liner when under the applied load was assumed to be governed by flexure. The liner's behavior could also have been governed by other global failure modes such as direct or diagonal shear, which would require modifications of the resistance function. Lastly, the mass of the liner was assumed to be uniform, which is a reasonable assumption in most cases that can also be adapted as necessary.

The next set of assumptions pertain to the load of the system. For this thesis I assumed that the load applied to the tunnel liner was uniformly distributed. This representation is accurate for a far-field, large charge. This does not mean that the load applied to the beam is limited to this configuration. For example, person borne improvised explosive devices (PBIEDs) that are close to the tunnel wall could be considered point or triangular loads. Under such loading, the possibility of spall and breach is higher, but it cannot be handled by a SDOF system.

The last set of limitations and assumptions pertain to the soil. One of the most important assumptions made was that of the effective depth of the soil. The effective depth of the soil was assumed to be constant throughout the length of the liner. Since the beam deflects more in the center than at the supports, the amount of soil mobilized will likely be different depending on the location along the beam. It was also assumed that only half of the soil in the effective depth was engaged. This meant that the calculation of

the inertial force only used half of the mass. Aside from the effective depth of the soil the nature of the soil also had to be considered. Soil by nature is nonlinear but in this thesis with the use of a secant modulus, it could be considered linear for simplicity. It may be of interest to consider whether the use of a shear modulus (G) instead of the Young's Modulus (E) is more appropriate. The conditions of the soil whether they are drained and undrained would be important to the response. In this case, due to the loading being fast, the assumption that the soil would be undrained seemed most appropriate. This would affect the soil stiffness because the water in the soil would take much more of the load. In regard to the stiffness of the soil, it was assumed to remain constant over the length of the liner. This followed the same assumptions made in previous practice cases. The mass of the soil was also kept constant over the length of the beam. These assumptions can be easily modified by reevaluating the relevant integrals. Improved soil assumptions are a possibility that could be explored, but it would be at the expense of model simplicity.

This thesis discussed how we could incorporate soil into an SDOF system and whether it was possible to get accurate a displacement result. Through some assumptions and an understanding of the limitations, it was possible to do so within reasonable values. There is still future work that can be done so that the times at which the peaks occur become identical. With that said, I believe this thesis is a step in the right direction and can be built upon in subsequent studies.

REFERENCES

Bai, F., Guo, Q., Root, K., Naito, C., and Quiel, S. (2018). "Blast Vulnerability Assessment of Road Tunnels with Reinforced Concrete Liners." Transp.Res.Rec., 2672(41), 156-164.

Bentz, E. (n.d.). “Hadrian Software Works.” *HADRIAN SOFTWARE WORKS*, <https://www.hadrianworks.com/> (Aug. 3, 2023).

Biggs, J.M. (1964). Introduction to Structural Dynamics, McGraw Hill, New York.

Chakraborty, T., Larcher, M., and Gebbeken, N. (2014). "Performance of Tunnel Lining Materials under Internal Blast Loading." International Journal of Protective Structures, 5(1), 83-96.

Choi, S., Wang, J., Munfakh, G., and Dwyre, E. (2012). "3D Nonlinear Blast Model Analysis for Underground Structures." GeoCongress 2006, 1-6.

Feldgun, V. R., Karinski, Y. S., and Yankelevsky, D. Z. (2014). "The effect of an explosion in a tunnel on a neighboring buried structure." Tunnel.Underground Space Technol., 44 42-55.

Goel, M. D., Verma, S., Mandal, J., and Panchal, S. (2021). "Effect of blast inside tunnel on surrounding soil mass, tunnel lining, and superstructure for varying shapes of tunnels." Underground Space, 6(6), 619-635.

Han, Y., Zhang, L., and Yang, X. (2016). "Soil-tunnel Interaction under Medium Internal Blast Loading." Procedia Engineering, 143 403-410.

Ranjit, K. C., Mishra, S., Chakraborty, T., and Matsagar, V. (2019). "Vulnerability analysis of tunnel linings under blast loading." International Journal of Protective Structures, 10(1), 73-94.

Roberts, J., Kulicki, J. M., Beranek, D. A., Englot, J. M., Fisher, J. W., Hungerbeeler, H., ... & Witt, K. (2003). Recommendations for Bridge and Tunnel Security (Report No. FHWA-IF-03-036). Federal Highway Administration (US).

Rodriguez-Nikl, Tonatiuh. (2023). “Theory for a Single Degree of Freedom Peak Displacement Analysis of a Tunnel Liner”. Zenodo.

Shin, J., Moon, H., and Chae, S. (2011). "Effect of blast-induced vibration on existing tunnels in soft rocks." Tunnel.Underground Space Technol., 26(1), 51-61.

U.S. Department of Defense (2008). Structures to Resist the Effects of Accidental Explosions, UFC 3- 340-02

Vesić, A.B. (1963). “Beams on Elastic Subgrade and the Winkler’s Hypothesis”, Proceedings of the 5th International Conference of Soil Mechanics, 845-850.

Zaghloul, A., Ranaweera, P., and Mohotti, D. (2018). "Assessment of Blast Effects on Passengers in Underground Trains." 25th Australian Conference on Mechanics of Structures and Materials (ACMSM25) Brisbane, Australia,